Building and Environment 216 (2022) 109000

Contents lists available at ScienceDirect

Building and Environment

journal homepage: www.elsevier.com/locate/buildenv

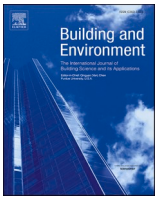

Contribution of urban functional zones to the spatial distribution of urban thermal environment

Yang Chen [a], Jun Yang [a,b,c,*], Ruxin Yang [a], Xiangming Xiao [d], Jianhong (Cecilia) Xia [e]

[a] Urban Climate and Human Settlements Research' Lab, JangHo Architecture, Northeastern University, Shenyang, 110169, China
[b] School of Humanities and Law, Northeastern University, Shenyang, 110169, China
[c] Human Settlements Research Center, Liaoning Normal University, Dalian, 110169, China
[d] Department of Microbiology and Plant Biology, Center for Spatial Analysis, University of Oklahoma, Norman, OK, 73019, USA
[e] School of Earth and Planetary Sciences (EPS), Curtin University, Perth, 65630, Australia

ARTICLE INFO

Keywords:
Land surface temperature
Urban thermal environment
Shenyang city
Urban functional zones

ABSTRACT

With the accelerated rate of urbanization, reasonable identification of urban functional zones has been increasingly important to urban development. In this study, we used OpenStreetMap and point of interest data combined with the classification standard of urban construction land, to identify the urban functional zones. In addition, Landsat 8 remote sensing images were utilized to retrieve land surface temperature, and the random forest algorithm was used to evaluate the contribution of different types of urban functional zones to the urban thermal environment. The results showed that the land surface temperature along Hunhe River in the central area of Shenyang gradually decreased. The temperature was high in the center of the experimental area and low in the north and south. Furthermore, in the main city zone of Shenyang, single functional zones accounted for 65.71% of the total study area, whereas mixed functional zones accounted for 34.29%. Among the various types of urban land, public service facility land contributed the most to the urban thermal environment with an impact of 21.65%, followed by residential, industrial, and commercial service facility lands, with impacts of 19.89%, 18.44%, and 17.58%, respectively. Additionally, the impact of road traffic land was 14.92%, whereas that of green square land was the lowest at 7.51%, 14.14% lower than that of public service facility land.

1. Introduction

Since the Industrial Revolution, urbanization has become an increasing trend worldwide. Urbanization refers to the process of transfer of the human living environment and social activities from the countryside to the city. Its main characteristics are massive flow of the rural population to cities and continuous expansion of urban spaces [1]. In the process of urbanization, the rapid increase of urban population and constant replacement of underlying natural urban surfaces by artificial surfaces have caused disordered expansion of urban land. This process causes variations in urban surface energy balance, resulting in the urban heat island effect [2–5]. The increased urban heat island effect causes, the urban thermal environment to deteriorate gradually, which not only affects the quality of urban human settlement and daily outdoor activities of residents, but also is closely related to urban energy consumption, ecosystem operation, vegetation phenology, and sustainable urban economy [6–9]. Therefore, qualitative and quantitative research on urban thermal environment issues is crucial for mitigating the urban heat island effect and thereby reducing health risks to humans [10].

The existing studies on the urban thermal environment focus mainly on the following aspects: formation and distribution characteristics of the urban thermal environment, driving mechanisms and influencing factors, and simulation and prediction [11–13]. Multi-faceted research on the urban thermal environment is important for understanding the urban climate, optimizing urban planning, and improving urban management and control mechanisms. The influencing factors of the urban thermal environment include spatial structure characteristics, land use/land cover, and landscape patterns [14–16]. During the process of urban expansion, the spatial structure is constantly changing, and the increase in building density hinders regional ventilation and the process of heat release [17]. Moreover, the urban surface cover has changed due to the transformation of land use types; natural landscapes have been replaced by artificial landscapes on a large scale, continuously increasing the roughness of the underlying urban surface. This leads to a

* Corresponding author. Urban Climate and Human Settlements Research' Lab, JangHo Architecture, Northeastern University, Shenyang, 110169, China
E-mail address: yangjun8@mail.neu.edu.cn (J. Yang).

https://doi.org/10.1016/j.buildenv.2022.109000
Received 21 January 2022; Received in revised form 16 March 2022; Accepted 17 March 2022
Available online 21 March 2022

decrease in the surface heat capacity and a higher heating rate in the city than in the surrounding areas [18]. In addition, the process of urbanization destroys the balance of the urban landscape pattern, leading to a decrease in the vegetation and water areas, which causes a reduction in evaporation and transpiration and affects the adjustment of regional temperature [19].

Although previous studies have described the spatial pattern and influencing factors of the urban thermal environment, the relationship between the urban thermal environment and its internal functional organization has not yet been established. Especially, the degree of influence of different urban functional zones on the thermal environment has not been explored. Urban functional zone refers to regional functional differentiation caused by the concentration of large amounts of similar human activities on limited urban land because of the influence of many factors such as nature, economy, history, and society in the process of urbanization [20,21]. The urban functional zones, which are constantly changing with social and economic development, are closely related to urban transportation, economy, and ecology [22–24]. Therefore, Therefore, it is important to optimize the urban functional structure by studying the influence of different urban functional zones on the urban thermal environment to help build a harmonious living environment [25,26]. This study was conducted in Shenyang City, China. We analyzed the spatial pattern of the urban thermal environment by adopting the random forest (RF) method to quantitatively study the contribution of different urban functional zones to it.

2. Literature review

2.1. Research scale

According to Oke T.R., the current quantitative research on the spatial distribution and influencing factors of urban thermal environment can be divided into meso-scale, local-scale and micro-scale in the spatial dimension [27]. Urban thermal environment research at different scales has different research objects and characteristics. Meso-scale research is suitable for exploring the spatial distribution of the thermal environment in urban planning areas, built-up areas, and central areas [28,29]. Local-scale research is more suitable to explore different spatial thermal environments, thermal comfort and anthropogenic heat in various urban functional areas or various land-use combinations [30–32]. The micro-scale focuses on the regional microclimate of urban built-up land, open spaces, and street canyons [33,34].

Reasonable classification of complex urban spaces is an important prerequisite for thermal environment research. Due to the addition of human activity data in the zoning process, urban functional zones effectively portray the relationship between people and land. Therefore, this study identifies the functional zones in the study area based on the local scale and explores the influence of urban functional zones on the heterogeneity of urban thermal environment distribution.

2.2. Data

This study uses land surface temperature (LST) to characterize the urban thermal environment. LST is an important variable used to characterize the land surface changes and the spatiotemporal pattern and influencing factors of the urban thermal environment [35]. With the development of remote sensing technology, the LST acquisition methods of LST have improved significantly. Compared with the traditional ground observation, remote sensing data has the advantages of convenient acquisition, low cost, and simultaneous coverage of a large area [36]. According to the spatial resolution setting of the satellite sensor, there are different retrieval methods, such as the single-window algorithm [37,38], split-window algorithm [39,40], multi-angle algorithm [41], and hyperspectral algorithm [42,43]. The single-window algorithm proposed by Qin Zhihao et al. [44] has a high retrieval accuracy and has been widely applied. In this study, the Landsat 8 OLI/TIRS image data was used to quantitatively invert the LST by using the single-window algorithm.

Traditional methods of urban functional zones identification use statistical data for analysis or expert scoring, which is highly subjective and results in inaccurate results. Recently, remote sensing technology has been widely used [45], and has demonstrated a great capability in depicting land parcels based on physical characteristics. However, it is not effective in identifying the spatial interaction between areas of human activity and their various functions [46]. Therefore, this study used road network data to divide the study area, combined the point of interest (POI) data representing human activities to identify urban functional zones, and attempted to combine human activities within urban functional space.

2.3. Method

To study the urban thermal environment, different methods are available based on different scales. In meso-scale research, the changes of urban net radiation, heat storage, sensible heat and latent heat are depicted by the spatial variability morphological characteristics, such as human activities, land use, and landscape patterns [47]. Micro-scale research focuses on the properties within the city, such as building forms and impervious surfaces. The influence of the surrounding microenvironment on the urban thermal environment is analyzed using simulation methods [48]. The research methods at the local-scale play a substantial role in the field of urban thermal environment research and have undergone continuous improvement and optimization. To explore the influence of different driving factors on the urban thermal environment, regression analysis such as the ordinary least squares model is commonly used [49]. These traditional regression methods ignore the spatial dependence of the data. To solve this problem, spatial regression models have been widely used [50,51]. The spatial regression model combines the attribute data with its position through spatial relationship and estimates the heat conduction and thermal interaction on the urban surface. However, because of the nonlinear relationships of the urban thermal environment, a machine learning model, the RF is applied. In this study, the RF algorithm was used to quantify the contribution of different urban functional zones to the urban thermal environment.

In summary, previous studies have analyzed the spatial pattern of the urban thermal environment and its related factors at different scales by using diverse indicators and methods, which laid a good foundation for subsequent research. However, the impact of the urban internal functional structure on the urban thermal environment has not been explored. Therefore, this study aimed to (1) examine the spatial heterogeneity of the thermal environment, (2) explore the spatial structure by identifying urban functional zones, and (3) study the specific impact of urban functional zones on the urban thermal environment. The results of this study provide urban planners and relevant department managers with insights for urban planning and management on how to optimize the urban functional structure to improve the urban thermal environment.

3. Study area and methodology

3.1. Study area

Shenyang, the capital of Liaoning Province, is in Northeast China and lies between 122°25′9″E, 41°11′51″N and 123°48′24″E, 43°2′13″N. It is a megacity and the core of the Shenyang metropolitan area which is under construction. Shenyang has a temperate semi-humid continental climate, with an average annual temperature of 6.2–9.7 °C and annual precipitation of 600–800 mm. Influenced by the monsoon, the precipitation is concentrated in summer. Further, as the temperature varies considerably, four distinct seasons are observed. As the political, economic, and cultural center as well as the transportation hub of the Northeast, Shenyang covers a total surface area of over 12,948 km^2. By

2020, the registered population of Shenyang was 7622 million, of which the urban population was 6202 million and the county (city) population was 1420 million. The study area comprised the central area of Shenyang, including five subdivisions (Dadong, Huanggu, Shenhe, Tiexi, and Heping), Yuhong District, Shenbei New District, Hunnan District, and Sujiatun District. The above-mentioned nine administrative districts are highly urbanized, so the most comprehensive functional zones that can reflect the characteristics of Shenyang's urban surface thermal environment to a certain extent are necessary. The specific extent and topographic features shown in the digital elevation model (DEM) of the selected study area is shown in Fig. 1.

3.2. Data sources and preprocessing

Landsat 8 OLI_TIRS image data (downloaded from the official website of the United States Geological Survey (USGS)) was used to retrieve information on LST. Considering the acquisition time of urban POI data and the quality of remote sensing images, the Landsat 8 image data on August 7, 2020 was selected, with an orbit number of 119 and a line number of 31. The satellite passed over the territory of the at approximately 10:28 a.m., while the cloud cover was less than 5%. The coverage area of the image included the study area and neighboring cities and counties.

This study utilized the road network (OpenStreetMap) and POI data to identify the urban functional zones. The road network data were obtained from the official website of OSM, which is currently the most popular platform that provides volunteered geographic information (VGI) [52]. The road network data included basic spatial information such as latitude and longitude, as well as information on attributes such as road names, road types, maximum driving speeds, and one-way streets. The POI data were obtained using the Amap API open data platform (accessed in April 2021). This study collected a total of 255,000 pieces of data for the study area comprising name, category, address, geographic coordinates, and other attributes (Table 1).

Firstly, meteorological parameters such as temperature, relative humidity and atmospheric pressure as the satellite transited the study area, were obtained from the historical weather query network (mip.lishi.tianqi.com). The Level 1T products of Landsat8 images were geometrically corrected based on terrain, and radiometric calibration and atmospheric correction operations were performed. As there were numerous messy, interrupted, and repeated lines in the OSM data, it was necessary to extend, delete and check the topology of the OSM road network data prior to conducting the analysis. The processed road network data were then converted into surfaces to generate irregular grids. Finally, a script was written and the crawling granularity was set to 0.05 to crawl the POI data in the study area using the Amap API. There were many types of POI data, and some existed in crossover situations; hence, operations such as elimination and completion, coordinate conversion, and avoidance of duplication were required. Moreover, the POI data were reclassified into six categories based on the national construction land classification standard (GB 50137-2011) and the national economic industry classification, each of which include several subcategories. Table 2 lists the specific classifications.

Table 1
Data source and description.

Data type	Resolution	Time	Data source
Landsat8 OLI_TIRS	30 m	2020.08.07	United States Geological Survey
Point of Interest Data	–	2021.04	AMAP Data Open Platform
Road Network Data	–	2020	OpenStreetMap
Vector Data	–	2020	National Geomatics Center of China

3.3. Methodology

This study retrieved the LST of the central area of Shenyang on August 7, 2020, using Landsat8 images. The weights of various POI data in different research units were calculated to determine the functional type of each research unit. Finally, the RF algorithm was used to evaluate the contribution of various urban functional zones to the urban thermal environment in each research unit. The research technology roadmap is provided in Fig. 2.

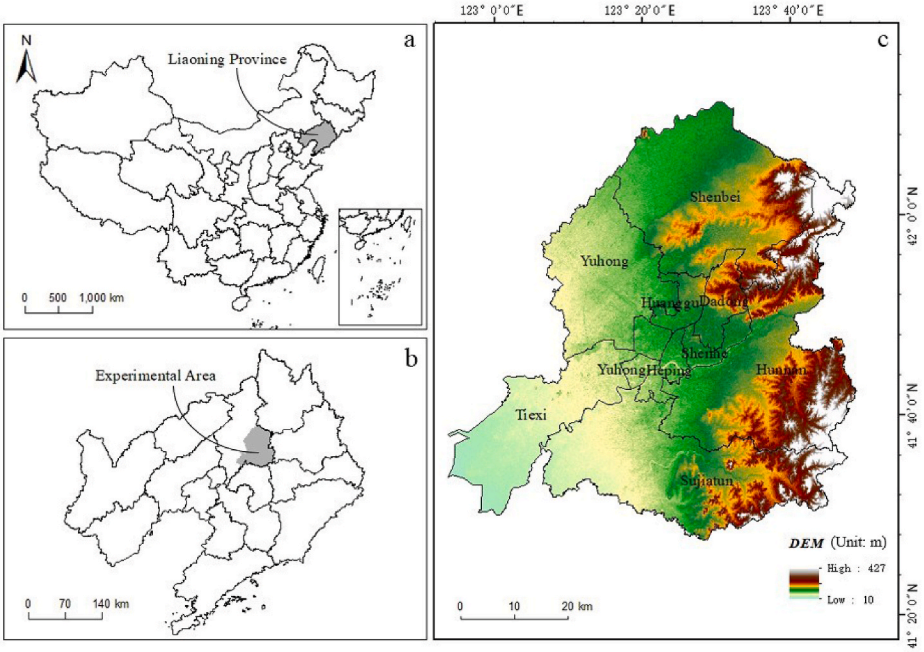

Fig. 1. Location of the study area (Shenyang, China). (a) Location of the Liaoning Province in China (b) Location of the study area in the Liaoning Province (c) The digital elevation model (DEM) of the study area.

Table 2
POI data classification.

Primary classification	Secondary classification	Quantity	Proportion
Residential	Business Residence, Accommodation Services	12717	6.83%
Industrial	Corporations	20290	10.90%
Commercial Service Facility	Catering Services, Sopping Services, Domestic Services, Financial Insurance Services	91976	49.40%
Public Service Facility	Public Utilities, Sports and Leisure services, Healthcare Services, Science, Education and Cultural Services, Government Agencies and Social Organizations	43844	23.55%
Green Square	Famous Tourist Sites	1361	0.73%
Road Traffic	Transportation Facility Services, Access Facilities, Road Ancillary Facilities	16013	8.60%

3.3.1. LST retrieval

The theoretical basis for retrieving the LST using remote sensing data comprises the heat radiation conduction equation quantified by Planck's law. Based on the spatial resolution of the satellite sensor, the inversion method was classified into four categories: 1) algorithm based on the radiation conduction equation [53], 2) single-band algorithm [37,54], 3) dual-band method (split window algorithm) [39], and 4) multi-band algorithm [55]. The 10th and 11th bands of Landsat8 are thermal infrared bands; however, owing to the high calibration uncertainty in the 11th band, the USGS does not recommend the split window algorithm. Instead, it recommends a single-band algorithm based on the 10th band to retrieve the LST [56]. The algorithm derived by Qin et al. [44,57] based on the surface radiation conduction equation, that used the sixth band was used to retrieve the LST. Atmospheric correction was not required when using this algorithm. The single-window algorithm is also suitable for ETM+ and Landsat8 data. The equation is as follows:

$$T_s = \{a_6(1 - C_6 - D_6) + (b_6(1 - C_6 - D_6) + C_6 + D_6)T_{sensor} - D_6 T_a\} / C_6 \quad (1)$$

where T_s is the brightness temperature of the sensor, T_a is the average temperature of the atmosphere, and a and b are the atmosphere function parameters. When the surface temperature was between 0 and 70 °C, c = -67.355351 and b = 0.458606. C and D are intermediate variables, which are calculated as follows:

$$C = \varepsilon\pi \quad (2)$$

$$D = (1 - \pi)[1 + (1 - \varepsilon)]\pi \quad (3)$$

In equations (2) and (3), ε is the land surface emissivity and π is the total atmospheric transmittance from the ground to the sensor.

3.3.2. Distribution of heat field levels

Quantitative analysis of the intensity of the LST was performed to effectively characterize the spatial distribution of the urban thermal environment and to calculate the contribution of different types of urban functional zones to the urban thermal environment. Therefore, it is necessary to classify the LST. The classification methods were divided into the equal interval method and the mean-standard deviation method. The mean-standard deviation method performs better than the equal interval method by considering the spatial distribution and a detailed depiction of the urban thermal environment [58]. This method uses a combination of the mean value of the surface temperature and multiples of different standard deviations to classify the intensity of the surface thermal field. Table 3 presents the specific classification levels. Based on the order of temperature from low to high, the surface thermal field intensities were classified as Class I, Class II, Class III, Class IV, Class V, and Class VI. Subsequently, they were assigned values from 1 to 6, which were called "surface thermal field values" here [59] based on the classification. A quantitative analysis of the relative intensity of the surface thermal environment was performed based on the surface thermal field values.

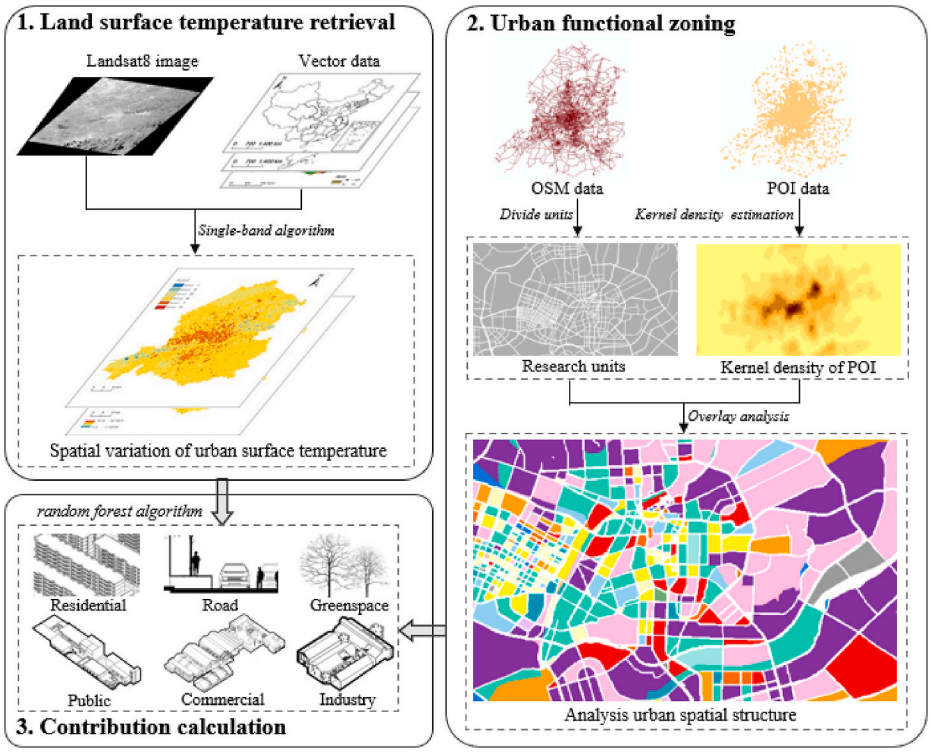

Fig. 2. Research technology roadmap.

Table 3
Usage of mean-standard deviation method to divide land surface thermal fields.

LST Level	Assignment	Meaning	LST Range
Class I	1	Low-temperature zone	$T_S < \mu - std$
Class II	2	Secondary moderate-temperature zone	$\mu - std \le T_S < \mu - 0.5std$
Class III	3	Moderate-temperature zone	$\mu - 0.5std \le T_S \le \mu$
Class IV	4	Secondary high-temperature zone	$\mu < T_S \le \mu + 0.5std$
Class V	5	High-temperature zone	$M + 0.5std < T_S \le \mu + std$
Class VI	6	Extreme high-temperature zone	$T_S > \mu + std$

Note: T_S is the inversion value of the LST, μ is the average value of the LST in the experimental area, and *std* is the standard deviation of the LST.

3.3.3. Urban functional zone identification

According to Yuan et al. [60], the method of identifying urban functional zones combined with OSM and POI data is high accurate, and provides an important reference for the analysis of urban spatial structure and urban functional zones. Therefore, this method was used to identify the urban functional zones.

First, OSM data were used to divide the city into different research units. After the topology correction for eliminating topological errors in the road network, the roads were divided into four levels, i.e., expressways and trunk roads comprised the first level, main roads comprised the second level, secondary roads comprised the third levels, and tertiary roads comprised the fourth level. Subsequently, the buffer zones were generated. The established road spaces were then removed from the study area to generate independent research units bound by the roads.

Second, various types of POI point data were connected to these research units. The POI point density of each urban functional area was calculated based on the POI point quadrat density method. The quadrat density [61–63] refers to the ratio of the number of POI data falling into the research unit divided by the area of each independent unit. The equation is as follows (unit: piece/km^2):

$$f(s) = \frac{n}{s} \tag{4}$$

where $f(s)$ is the quadrat density, n is the number of POI data in each sample square, and s is the area of a sample square.

When identifying the urban functional zones, if the density value of a certain type of POI point in a certain unit accounted for 50% or more of the total density value, this unit was a single functional zone. Furthermore, if there were two types of POI points in a certain unit accounting for 20–50% of the total density value, this unit was a mixed zone of the two types of POI. Moreover, if the density value of all types of POI in a certain unit was zero, such a unit was deemed to be a no-data area, whereas the rest of the units were defined as mixed functional zones.

3.3.4. Statistical analysis

First, to calculate the contribution of each urban functional zone to the LST, zonal statistics analysis was used to count the number of functional zones in the study area (Table 5). Second, a one-way analysis of variance (ANOVA) was performed between the various functional zones and the LST to estimate the variation of the LST among different urban functional zones.

Third, the RF algorithm was used to evaluate the contribution. The RF algorithm is a newly emerging and highly flexible machine learning algorithm, which is widely used in regression and classification [64]. This algorithm integrates multiple trees through an ensemble learning method, a large branch of machine learning [65], and collects the results by randomly selecting features from each decision tree, finally adopting majority voting or averages according to each specific problem with the results in the form of stable and accurate predictions [66]. The algorithm has many advantages, such as simple implementation, high accuracy, and strong resistance to overfitting [67].

Table 4
Statistics of land surface temperature levels.

LST Level	Meaning	Quantity	Proportion
Class I	Low-temperature zone	4093	0.10
Class II	Secondary moderate-temperature zone	100741	2.48
Class III	Moderate-temperature zone	636829	15.68
Class IV	Secondary high-temperature zone	2851240	70.20
Class V	High-temperature zone	468854	11.54
Class VI	Extreme high-temperature zone	15	0

4. Results

4.1. Spatial distribution of the surface thermal environment in Shenyang

In this study, we used Landsat 8 OLI_TIRS images to retrieve the LST of the central area of Shenyang on August 7, 2020 based on the single-window algorithm, the results of which are shown in Fig. 3. The study area is dominated by plains. Previous studies have shown that in areas in which the ground was relatively flat, the temperature observed at the weather observation station was closely related to the true LST, and could compare with the LST retrieved from satellite data on the pixel scale. The actual temperature observed at the meteorological station when the Landsat8 satellite passed the study area on August 7, 2020 was considered the true value. The root mean square error (RMSE) of the retrieved LST in the study area was less than 1k, which showed that the result of the LST retrieval was considered reliable.

Fig. 4 shows the results of using the mean-standard deviation method to classify the surface thermal field. The average surface temperature was 28.39 °C, and the standard deviation was 6.04 °C. The estimated temperatures of Huanggu district, Dadong district, the southern part of Yuhong district, Heping district, the northern part of Tiexi district and the western part of Shenhe district were higher than those of other areas. Generally, the surface temperature in the central area of Shenyang decreased gradually to the north and south of the Hunhe River. The average thermal field level in the north of the Hunhe River was higher than that in the south.

The number of LST levels were counted to quantitatively indicate the relative intensity of the surface temperature, the results of which are

Table 5
Surface temperature distribution in different types of urban functional zone.

Functional zone type	n	$\bar{x} \pm s$	F	P
Road	26	32.32 ± 4.22	3.006	<0.05
Industrial	190	32.04 ± 4.94		
Industrial-Road	4	32.23 ± 2.90		
Industrial-Public	52	33.52 ± 3.66		
Public	217	34.30 ± 4.24		
Public-Road	18	33.19 ± 3.48		
Public-Green square	4	30.70 ± 6.99		
Residential	102	34.54 ± 4.46		
Residential-Road	6	33.68 ± 1.05		
Residential-Industrial	89	32.56 ± 3.89		
Residential-Public	64	34.19 ± 4.64		
Residential-Commercial	35	34.00 ± 2.96		
Green square	11	31.49 ± 4.32		
Commercial	299	32.75 ± 4.09		
Commercial-Road	6	33.01 ± 5.25		
Commercial-Public	120	32.88 ± 4.95		
Commercial-Green square	2	32.26 ± 5.74		
Comprehensive Functional Area	41	32.89 ± 5.60		

Note: n is the number of units corresponding to the functional zones, $\bar{x}$ is the average value of the surface temperature, and s is the standard deviation of the surface temperature.

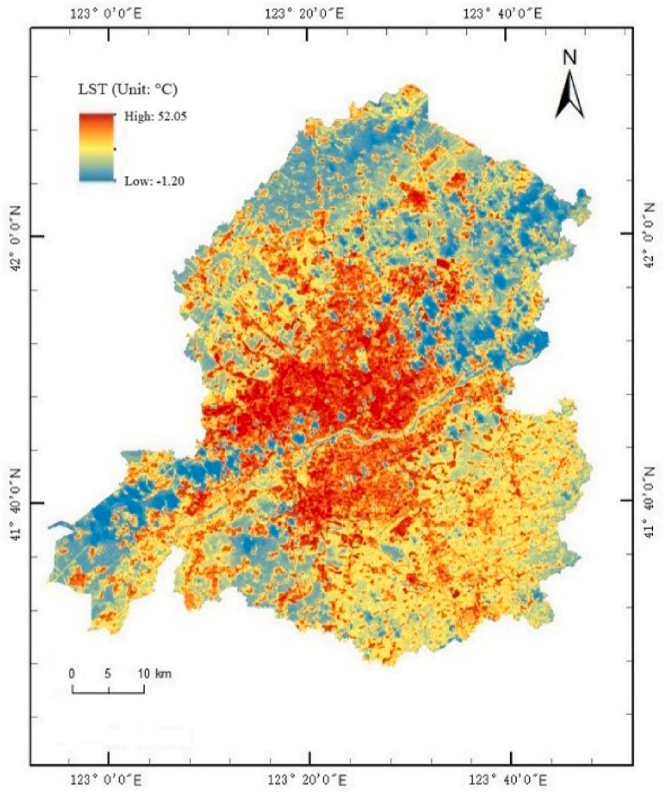

Fig. 3. LST in Shenyang.

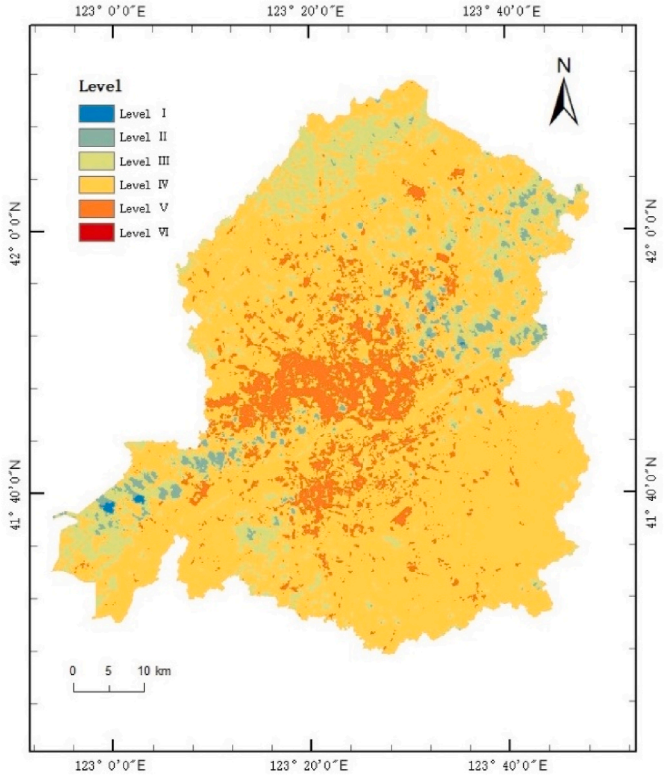

Fig. 4. Spatial distribution of LST levels in Shenyang.

shown in Table 4. The surface thermal field levels of the central area of Shenyang were mainly concentrated in the moderate-temperature, secondary high-temperature, and high-temperature zones. Here, the high-temperature zones accounted for more than 80% of the total area. Simultaneously, there was a considerably low distribution of the low-temperature and extreme high-temperature zones.

4.2. Identification of the spatial structure of Shenyang

To identify the urban functional zones, 1286 independent units in the central area of Shenyang were obtained. Then, the quadrat density of various types of POI data in each independent unit was calculated; the results are shown in Fig. 5. Commercial service facility land including single commercial service facility land, and commercial-public mixed land, was the most widely distributed, accounting for 44.36% of the total area; moreover, it was evenly distributed within the study area. Public service facility land and industrial land followed next, accounting for 32.62% of the total area. Public land was mainly distributed in the center of the study area, whereas industrial land was mainly distributed outside the second ring road of Shenyang. Residential land which accounted for 20.36% of the total area and was, mainly distributed in the center of the study area.

4.3. Spatial interaction between various urban activity environments and the surface thermal environment in Shenyang

To explore the impact of various urban activities on the surface thermal environment, a one-way ANOVA was conducted between the various functional zones and the urban surface temperature of the study area. The variance analysis showed a significance >0.05, indicating that the variance was homogeneous and could be utilized. The significance of the variance analysis was set to $P < 0.05$. Thus, a P value of <0.05 indicated the existence of significant differences between different functional areas and urban surface temperatures. Table 5 lists the results of the specific analysis. Public service facility, residential, commercial service facility, and road traffic lands had a higher impact on the surface thermal environment than industrial and green square lands.

To further quantify the impact of different functional zones on the urban surface temperature, the RF algorithm was used to evaluate the contribution of various human activities to the urban thermal environment (Table 6). The RF algorithm is characterized by its high efficiency and flexibility, relatively accurate classification accuracy, and strong anti-noise ability [68]. To obtain the optimal parameters of the RF model, the grid search tool GridSearchCV was used to determine the best parameters to achieve the optimal classification performance. The parameters are as follows: n_estimators = 127, bootstrap = True, criterion = 'entropy', max_features = 6, min_samples_leaf = 1, min_samples_split

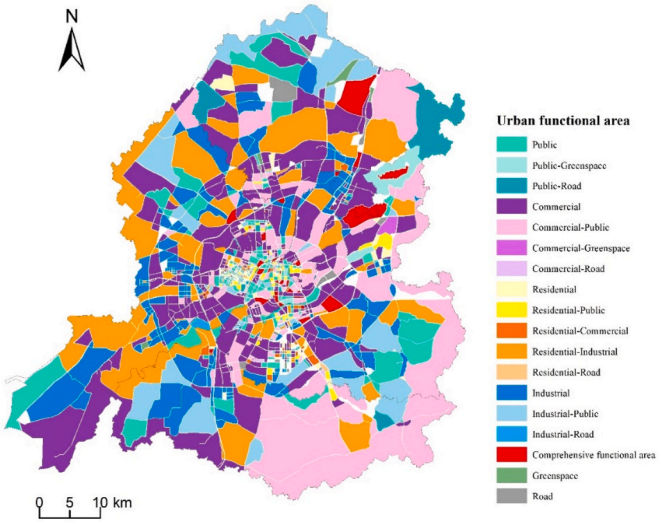

Fig. 5. Recognition results of functional zones in downtown Shenyang.

Table 6
The contribution of different urban functions to the urban thermal environment.

Urban Function Type	Contribution to the Surface Thermal Field
Public	21.65%
Residential	19.89%
Industrial	18.44%
Commercial	17.58%
Road	14.92%
Green square	7.51%

= 2. The best average accuracy obtained using the grid search method based on the ten-fold cross-validation is 0.872. For different urban functional zones formed by various human activities, the highest impact on the surface thermal environment was contributed by public service facility land followed by residential land, industrial land, commercial service facility land, road traffic land, and green square land in that order (Table 6).

5. Discussion

5.1. Quantitative measure of spatial distribution of the urban thermal environment

This study carried out a quantitative measurement of the urban thermal environment by inverting the LST and thus revealed the spatial pattern of the urban thermal environment. Previous studies have shown that the spatial distribution of the urban thermal environment is related to the changes in impervious surfaces [68,69], changes in land use/land cover [70–72], urban landscape patterns [73–76], urban expansion [77,78], and vegetation and water bodies [79–81]. However, the spatial variation of the urban thermal environment based on urban functional zoning has not been studied in detail. In this study, the OSM and POI data were combined to identify the urban functional zones, which could eliminate land use data to detect the internal thermal environment of different functional units. In this study, the Landsat8 OLI_TIRS image data were used to invert the LST of the study area, and the mean-standard deviation method is used to classify the LSTs, a quantitative measurement of the urban thermal environment. The results provide a new perspective for studying the spatial variation of the urban thermal environment, and references for regional functional zoning and urban planning.

5.2. Contribution of different urban activity environment to the urban thermal environment

The results showed that the contribution of different urban functional zones to the urban thermal environment varied significantly. Previous studies have focused on the impact of land use/cover changes on the urban thermal environment. Land use/cover plays an important role in the changes of the environmental and sustainable development, and its change is a dynamic process. Studies have shown that land use/cover has a significant impact on urban heat island intensity. Farmland and forest can help cities to cool down; the cooling effect of farmland and forests is related to their distribution and composition [82]. However, the previous studies did not consider the influence of human activities on the thermal environment. Therefore, this study explored the impact of urban functional zones, which were divided based on human activities, on the urban thermal environment.

Research results showed that the land used for public service facilities had the highest contribution to the thermal environment as it constituted 21.65% of the total land. The contribution of residential, industrial, and commercial service facility lands to the thermal environment was less than that of public service facility land, constituting 19.89%, 18.44%, and 17.58%, respectively. According to Gao et al. [67], the average LST of industrial and manufacturing, and commercial and business facility lands in Wuhan was higher than that of administration and public services, and residential lands. However, the opposite conclusion was reached in this study. The reason for this phenomenon might be due to the following. On the one hand, Wuhan was a city with a high proportion of heavy industry in 2013, and its industrial heat production was very serious. Although Shenyang was once a city of heavy industry, in response to the national policy of ecological environment construction, it completed the industrial transformation of heavy industry and employment adjustment by 2020. The proportion of the secondary sector has been decreasing, and the proportion of the tertiary sector has been increasing there. On the other hand, the time of datasets selected in this study were all post 2020, while the datasets used by Gao et al. were collected in 2013. During this period, COVID-19 was rampant, so people's lifestyle affected by the policy was considerably different to previously. Therefore, the heat generated by the flow of people on public service facility land represented by public facilities and health care services increased significantly. In addition, because of the anti-epidemic policy, people consciously reduced unnecessary outings, which led to higher anthropogenic heat in residential areas than over a normal period. Meanwhile, industrial production and commercial activities were shutdown to some extent during the COVID-19 period, resulting in a significant decline in anthropogenic heat.

5.3. Limitations

There are some limitations in this study that need further discussion and resolution. First, urban functional zoning is affected by many factors, including physical geography, social economy, and human activities. The OSM and POI data used here only help to study the division of urban functional zones based on transportation networks and human activities. Hence, to obtain more accurate classification results, more open datasets, high-resolution remote sensing images that can represent urban spaces, and statistical data to describe population movements should be added in the future. Second, owing to the lack of datasets, the time series of the spatial variation of the urban thermal environment based on functional zoning was not included in the analysis. Therefore, in the future, time series analysis will be incorporated, such as the differences in the contribution of urban functional zones to the urban thermal environment in different seasons or the evolutionary law of the contribution of urban functional zones to the urban thermal environment.

6. Conclusions

As the effects of urban heat islands are becoming more severe, quantitative research on the impact of various urban functional zones on the urban thermal environment helps to effectively reflect the impact of various human activities on the formation of urban heat islands. Landsat 8 data were used to retrieve the surface temperature of the study area along with OSM and POI data to quantitatively identify urban functional zones. The heterogeneity of the spatial distribution of the urban thermal environment was studied based on functional zoning. The main conclusions of this study were as follows:

(1) The surface temperature of the study area was mostly distributed in the moderate-temperature zone, secondary high-temperature zone, and high-temperature zone. The number of urban land units considering these three thermal field levels accounted for 97.22% of the total study area. Additionally, the secondary moderate-temperature zone accounted for 2.48% of the total area. Moreover, there was almost no distribution of the low-temperature and extreme high-temperature zones. The areas with higher temperatures included Huanggu district, Dadong district, the southern part of Yuhong district, Heping district, the northern part of Tiexi district and the western part of Shenhe district. Overall, the surface temperature in the central area of

Shenyang decreased gradually in both, the northern and southern directions along the Hunhe River, and the average thermal field level in the north of the Hunhe River was higher than in the south.

(2) Commercial service facilities were most widely distributed in the central urban area of Shenyang, followed by industrial and public service facility lands, whereas residential land accounted for a relatively small proportion. Further, single functional zones accounted for 65.71%, whereas the land with two or more functions accounted for 34.29% of the total study area.

(3) Among the various types of urban land, the highest to the lowest impacts on the surface thermal environment were contributed by public service facility, residential, industrial, commercial service facility, road traffic, and green square lands in the order. The specific contributions are 21.65%, 19.89%, 18.44%, 17.58%, 14.92%, and 7.51%. As various constructions contribute more than 90% to the urban thermal environment, governments, planning departments and other relevant units should plan land use rationally, and improve the urban thermal environment by increasing the green space to realize sustainable urban development.

CRediT authorship contribution statement

Yang Chen: Data curation, Software, Writing – original draft, Writing – review & editing. **Jun Yang:** Writing – review & editing, Methodology, Conceptualization. **Ruxin Yang:** Writing – review & editing, Data curation. **Xiangming Xiao:** Writing – review & editing. **Jianhong (Cecilia) Xia:** Writing – review & editing.

Declaration of competing interest

The authors declare that they have no known competing financial interests or personal relationships that could have appeared to influence the work reported in this paper.

Acknowledgements

The authors would like to acknowledge all colleagues and friends who have voluntarily reviewed the translation of the survey and the manuscript of this study. This research study was supported by the National Natural Science Foundation of China (grant nos. 41771178 and 42030409), the Fundamental Research Funds for the Central University (grant no. N2111003), the Second Tibetan Plateau Scientific Expedition and Research Program (STEP) (grant no. 2019QZKK1004), and the Innovative Talents Support Program of Liaoning Province (Grant No. LR2017017).

References

[1] L. Bertinelli, D. Black, Urbanization and growth, J. Urban Econ. 56 (2004) 80–96, https://doi.org/10.1016/j.jue.2004.03.003.

[2] Y. Li, S. Schubert, J.P. Kropp, D. Rybski, On the influence of density and morphology on the Urban Heat Island intensity, Nat. Commun. 11 (2020) 2647, https://doi.org/10.1038/s41467-020-16461-9.

[3] X. Zhang, Y. Sun, Investigating institutional integration in the contexts of Chinese city-regionalization: evidence from Shenzhen–Dongguan–Huizhou, Land Use Pol. 88 (2019), 104170, https://doi.org/10.1016/j.landusepol.2019.104170.

[4] X. Li, Y. Zhou, G.R. Asrar, M. Imhoff, X. Li, The surface urban heat island response to urban expansion: a panel analysis for the conterminous United States, Sci. Total Environ. 605–606 (2017) 426–435, https://doi.org/10.1016/j.scitotenv.2017.06.229.

[5] T. Panagopoulos, J.A. González Duque, M. Bostenaru Dan, Urban planning with respect to environmental quality and human well-being, Environ. Pollut. 208 (2016) 137–144, https://doi.org/10.1016/j.envpol.2015.07.038.

[6] H. Akbari, M. Pomerantz, H. Taha, Cool surfaces and shade trees to reduce energy use and improve air quality in urban areas, Sol. Energy 70 (2001) 295–310, https://doi.org/10.1016/S0038-092X(00)00089-X.

[7] J. Yang, J. Ren, D. Sun, X. Xiao, J. (Cecilia) Xia, C. Jin, X. Li, Understanding land surface temperature impact factors based on local climate zones, Sustain. Cities Soc. 69 (2021), 102818, https://doi.org/10.1016/j.scs.2021.102818.

[8] B.-J. He, D. Zhao, K. Xiong, J. Qi, G. Ulpiani, G. Pignatta, D. Prasad, P. Jones, A framework for addressing urban heat challenges and associated adaptive behavior by the public and the issue of willingness to pay for heat resilient infrastructure in Chongqing, China, Sustain. Cities Soc. 75 (2021), 103361, https://doi.org/10.1016/j.scs.2021.103361.

[9] B.-J. He, J. Wang, H. Liu, G. Ulpiani, Localized synergies between heat waves and urban heat islands: implications on human thermal comfort and urban heat management, Environ. Res. 193 (2021), 110584, https://doi.org/10.1016/j.envres.2020.110584.

[10] J. Yang, J. Sun, Q. Ge, X. Li, Assessing the impacts of urbanization-associated green space on urban land surface temperature: a case study of Dalian, China, Urban For. Urban Green. 22 (2017) 1–10, https://doi.org/10.1016/j.ufug.2017.01.002.

[11] A. Mohajerani, J. Bakaric, T. Jeffrey-Bailey, The urban heat island effect, its causes, and mitigation, with reference to the thermal properties of asphalt concrete, J. Environ. Manag. 197 (2017) 522–538, https://doi.org/10.1016/j.jenvman.2017.03.095.

[12] Z. Li, L. Liu, X. Dong, J. Liu, The study of regional thermal environments in urban agglomerations using a new method based on metropolitan areas, Sci. Total Environ. 672 (2019) 370–380, https://doi.org/10.1016/j.scitotenv.2019.03.486.

[13] J. Yang, Y. Yang, D. Sun, C. Jin, X. Xiao, Influence of urban morphological characteristics on thermal environment, Sustain. Cities Soc. 72 (2021), 103045, https://doi.org/10.1016/j.scs.2021.103045.

[14] Y. Zhang, H. Balzter, Y. Li, Influence of impervious surface area and fractional vegetation cover on seasonal urban surface heating/cooling rates, Rem. Sens. 13 (2021) 1263, https://doi.org/10.3390/rs13071263.

[15] W. Yue, S. Qiu, H. Xu, L. Xu, L. Zhang, Polycentric urban development and urban thermal environment: a case of Hangzhou, China, Landsc. Urban Plann. 189 (2019) 58–70, https://doi.org/10.1016/j.landurbplan.2019.04.008.

[16] L. Yao, Y. Xu, B. Zhang, Effect of urban function and landscape structure on the urban heat island phenomenon in Beijing, China, Landsc. Ecol. Eng. 15 (2019) 379–390, https://doi.org/10.1007/s11355-019-00388-5.

[17] Z. Xu, Z. Cai, S. Su, M. Kang, Y. Ge, Unraveling the association between the urban polycentric structure and urban surface thermal environment in urbanizing China, Sustain. Cities Soc. 76 (2022), 103490, https://doi.org/10.1016/j.scs.2021.103490.

[18] P.Y. Fan, K.P. Chun, A. Mijic, D.N.-Y. Mah, Q. He, B. Choi, C.K.C. Lam, O. Yetemen, Spatially-heterogeneous impacts of surface characteristics on urban thermal environment, a case of the Guangdong-Hong Kong-Macau Greater Bay Area, Urban Clim. 41 (2022), 101034, https://doi.org/10.1016/j.uclim.2021.101034.

[19] L. Zhou, F. Hu, B. Wang, C. Wei, D. Sun, S. Wang, Relationship between urban landscape structure and land surface temperature: spatial hierarchy and interaction effects, Sustain. Cities (2022) 1–12.

[20] Y. Chen, X. Liu, X. Li, X. Liu, Y. Yao, G. Hu, X. Xu, F. Pei, Delineating urban functional areas with building-level social media data: a dynamic time warping (DTW) distance based k-medoids method, Landsc. Urban Plann. 160 (2017) 48–60, https://doi.org/10.1016/j.landurbplan.2016.12.001.

[21] X. Liu, L. Ma, X. Li, B. Ai, S. Li, Z. He, Simulating urban growth by integrating landscape expansion index LEI and cellular automata, Int. J. Geogr. Inf. Sci. 28 (2014) 148–163, https://doi.org/10.1080/13658816.2013.831097.

[22] X. Guan, H. Wei, S. Lu, Q. Dai, H. Su, Assessment on the urbanization strategy in China: achievements, challenges and reflections, Habitat Int. 71 (2018) 97–109, https://doi.org/10.1016/j.habitatint.2017.11.009.

[23] S. Abdullahi, B. Pradhan, S. Mansor, A.R.M. Shariff, GIS-based modeling for the spatial measurement and evaluation of mixed land use development for a compact city, GIScience Remote Sens. 52 (2015) 18–39, https://doi.org/10.1080/15481603.2014.993854.

[24] F. Wang, W. Dong, Z. Zhao, H. Wang, W. Li, G. Chen, F. Wang, Y. Zhao, J. Huang, T. Zhou, Heavy metal pollution in urban river sediment of different urban functional areas and its influence on microbial community structure, Sci. Total Environ. 778 (2021), 146383, https://doi.org/10.1016/j.scitotenv.2021.146383.

[25] B.-J. He, L. Ding, D. Prasad, Relationships among local-scale urban morphology, urban ventilation, urban heat island and outdoor thermal comfort under sea breeze influence, Sustain. Cities Soc. 60 (2020), 102289, https://doi.org/10.1016/j.scs.2020.102289.

[26] A. Sharifi, M. Pathak, C. Joshi, B.-J. He, A systematic review of the health co-benefits of urban climate change adaptation, Sustain. Cities Soc. 74 (2021), 103190, https://doi.org/10.1016/j.scs.2021.103190.

[27] T.R. Oke, G. Mills, A. Christen, J.A. Voogt, Urban Climates, Cambridge University Press, 2017. https://ideas.repec.org/b/cup/cbooks/9781107429536.html. (Accessed 21 December 2021).

[28] L. Sheng, X. Tang, H. You, Q. Gu, H. Hu, Comparison of the urban heat island intensity quantified by using air temperature and Landsat land surface temperature in Hangzhou, China, Ecol. Indicat. 72 (2017) 738–746, https://doi.org/10.1016/j.ecolind.2016.09.009.

[29] P. Vahmani, G.A. Ban-Weiss, Impact of remotely sensed albedo and vegetation fraction on simulation of urban climate in WRF-urban canopy model: a case study of the urban heat island in Los Angeles, J. Geophys. Res. Atmos. 121 (2016) 1511–1531, https://doi.org/10.1002/2015JD023718.

[30] L. Liu, Y. Lin, J. Liu, L. Wang, D. Wang, T. Shui, X. Chen, Q. Wu, Analysis of local-scale urban heat island characteristics using an integrated method of mobile measurement and GIS-based spatial interpolation, Build. Environ. 117 (2017) 191–207, https://doi.org/10.1016/j.buildenv.2017.03.013.

[31] A. Dimoudi, A. Kantzioura, S. Zoras, C. Pallas, P. Kosmopoulos, Investigation of urban microclimate parameters in an urban center, Energy Build. 64 (2013) 1–9, https://doi.org/10.1016/j.enbuild.2013.04.014.

[32] Z. Zhao, A. Sharifi, X. Dong, L. Shen, B.-J. He, Spatial variability and temporal heterogeneity of surface urban heat island patterns and the suitability of local climate zones for land surface temperature characterization, Rem. Sens. 13 (2021) 4338, https://doi.org/10.3390/rs13214338.
[33] F. Bourbia, F. Boucheriba, Impact of street design on urban microclimate for semi arid climate (Constantine), Renew. Energy 35 (2010) 343–347, https://doi.org/10.1016/j.renene.2009.07.017.
[34] D. Shi, J. Song, J. Huang, C. Zhuang, R. Guo, Y. Gao, Synergistic cooling effects (SCEs) of urban green-blue spaces on local thermal environment: a case study in Chongqing, China, Sustain. Cities Soc. 55 (2020), 102065, https://doi.org/10.1016/j.scs.2020.102065.
[35] Isabel F. Trigo, Isabel T. Monteiro, Folke Olesen, An assessment of remotely sensed land surface temperature, J. Geophys. Res. Atmos. (2008), https://doi.org/10.1029/2008JD010035. Ewa.
[36] Q. Weng, Remote sensing of impervious surfaces in the urban areas: requirements, methods, and trends, Remote Sens. Environ. 117 (2012) 34–49, https://doi.org/10.1016/j.rse.2011.02.030.
[37] Z. Qin, A. Karnieli, P. Berliner, A mono-window algorithm for retrieving land surface temperature from Landsat TM data and its application to the Israel-Egypt border region, Int. J. Rem. Sens. 22 (2001) 3719–3746, https://doi.org/10.1080/01431160010006971.
[38] J.C. Price, Estimating surface temperatures from satellite thermal infrared data—a simple formulation for the atmospheric effect, Remote Sens. Environ. 13 (1983) 353–361, https://doi.org/10.1016/0034-4257(83)90036-6.
[39] Z. Wan, J. Dozier, A generalized split-window algorithm for retrieving land-surface temperature from space, IEEE Trans. Geosci. Rem. Sens. 34 (1996) 892–905, https://doi.org/10.1109/36.508406.
[40] C. Coll, V. Caselles, J.A. Sobrino, E. Valor, On the atmospheric dependence of the split-window equation for land surface temperature, Int. J. Rem. Sens. 15 (1994) 105–122, https://doi.org/10.1080/01431169408954054.
[41] A.J. Prata, Land surface temperatures derived from the advanced very high resolution radiometer and the along-track scanning radiometer: 1. Theory, J. Geophys. Res. Atmos. 98 (1993) 16689–16702, https://doi.org/10.1029/93JD01206.
[42] N. Wang, H. Wu, F. Nerry, C. Li, Z.-L. Li, Temperature and emissivity retrievals from hyperspectral thermal infrared data using linear spectral emissivity constraint, IEEE Trans. Geosci. Rem. Sens. 49 (2011) 1291–1303, https://doi.org/10.1109/TGRS.2010.2062527.
[43] C. Borel, Error analysis for a temperature and emissivity retrieval algorithm for hyperspectral imaging data, Int. J. Rem. Sens. 29 (2008) 5029–5045, https://doi.org/10.1080/01431160802036540.
[44] Z.M. hua Qin Zhi hao, Mono-window algorithm for retrieving land surface temperature from landsat TM6 data, J. Geogr. Sci. 56 (2001) 456–466, https://doi.org/10.11821/xb200104009.
[45] S. Hu, L. Wang, Automated urban land-use classification with remote sensing, Int. J. Rem. Sens. 34 (2013) 790–803, https://doi.org/10.1080/01431161.2012.714510.
[46] Y. Zhang, Q. Li, W. Tu, K. Mai, Y. Yao, Y. Chen, Functional urban land use recognition integrating multi-source geospatial data and cross-correlations, Comput, Environ. Urban Syst. 78 (2019), 101374, https://doi.org/10.1016/j.compenvurbsys.2019.101374.
[47] G. Guo, Z. Wu, R. Xiao, Y. Chen, X. Liu, X. Zhang, Impacts of urban biophysical composition on land surface temperature in urban heat island clusters, Landsc. Urban Plann. 135 (2015) 1–10, https://doi.org/10.1016/j.landurbplan.2014.11.007.
[48] M. Bruse, H. Fleer, Simulating surface–plant–air interactions inside urban environments with a three dimensional numerical model, Environ. Model. Software 13 (1998) 373–384, https://doi.org/10.1016/S1364-8152(98)00042-5.
[49] M. Morabito, A. Crisci, A. Messeri, S. Orlandini, A. Raschi, G. Maracchi, M. Munafò, The impact of built-up surfaces on land surface temperatures in Italian urban areas, Sci. Total Environ. 551–552 (2016) 317–326, https://doi.org/10.1016/j.scitotenv.2016.02.029.
[50] X. Yang, W. Jin, GIS-based spatial regression and prediction of water quality in river networks: a case study in Iowa, J. Environ. Manag. 91 (2010) 1943–1951, https://doi.org/10.1016/j.jenvman.2010.04.011.
[51] J.-H. Kim, D. Gu, W. Sohn, S.-H. Kil, H. Kim, D.-K. Lee, Neighborhood landscape spatial patterns and land surface temperature: an empirical study on single-family residential areas in Austin, Texas, Int. J. Environ. Res. Publ. Health 13 (2016) E880, https://doi.org/10.3390/ijerph13090880.
[52] Y. Hong, Y. Yao, Hierarchical community detection and functional area identification with OSM roads and complex graph theory, Int. J. Geogr. Inf. Sci. 33 (2019) 1569–1587, https://doi.org/10.1080/13658816.2019.1584806.
[53] R.S. Chatterjee, N. Singh, S. Thapa, D. Sharma, D. Kumar, Retrieval of land surface temperature (LST) from landsat TM6 and TIRS data by single channel radiative transfer algorithm using satellite and ground-based inputs, Int. J. Appl. Earth Obs. Geoinform. 58 (2017) 264–277, https://doi.org/10.1016/j.jag.2017.02.017.
[54] J.C. Jiménez-Muñoz, J.A. Sobrino, A generalized single-channel method for retrieving land surface temperature from remote sensing data, J. Geophys. Res. Atmos. 108 (2003), https://doi.org/10.1029/2003JD003480.
[55] Z.-L. Li, F. Becker, Feasibility of land surface temperature and emissivity determination from AVHRR data, Remote Sens. Environ. 43 (1993) 67–85, https://doi.org/10.1016/0034-4257(93)90065-6.
[56] J.A. Barsi, J.R. Schott, S.J. Hook, N.G. Raqueno, B.L. Markham, R.G. Radocinski, Landsat-8 thermal infrared sensor (TIRS) vicarious radiometric calibration, Rem. Sens. 6 (2014) 11607–11626, https://doi.org/10.3390/rs61111607.
[57] J. Yang, Y. Zhan, X. Xiao, J.C. Xia, W. Sun, X. Li, Investigating the diversity of land surface temperature characteristics in different scale cities based on local climate zones, Urban Clim. 34 (2020), 100700, https://doi.org/10.1016/j.uclim.2020.100700.
[58] S. Chen, T. Wang, Comparison analyses of equal interval method and mean-standard deviation method used to delimitate urban Heat Island, Geo Inf. Sci. 11 (2009) 145–150, https://doi.org/10.3724/SP.J.1047.2009.00145.
[59] Z. Yang, Y. Chen, Z. Wu, How urban expansion affects the thermal environment? A study of the impact of natural cities on the thermal field value and footprint of thermal environment, Ecol. Indicat. 126 (2021), 107632, https://doi.org/10.1016/j.ecolind.2021.107632.
[60] Y. Zhang, Q. Li, H. Huang, W. Wu, X. Du, H. Wang, The combined use of remote sensing and social sensing data in fine-grained urban land use mapping: a case study in Beijing, China, Rem. Sens. 9 (2017) 865, https://doi.org/10.3390/rs9090865.
[61] J. Chi, L. Jiao, T. Dong, Y. Gu, Y. Ma, Quantitative identification and visualization of urban functional area based on POI data. https://doi.org/10.14188/j.2095-6045.2016.02.017, 2016, 41,68-73.
[62] W. Yu, T. Ai, The visualization and analysis of POI features under network space supported by Kernel density estimation, Cehui XuebaoActa Geod. Cartogr. Sin. 44 (2015) 82–90, https://doi.org/10.11947/j.AGCS.2015.20130538.
[63] Y. Huang, S. Shao, Y. Lei, J. Tian, Identification of urban functional zones using network Kernel density estimation and Kriging interpolation, J. Geom. (2019). http://en.cnki.com.cn/Article_en/CJFDTotal-CHXG201904003.htm. (Accessed 10 December 2021).
[64] L. Breiman, Random forests, Mach. Learn. 45 (2001) 5–32, https://doi.org/10.1023/A:1010933404324.
[65] Y. Xu, A. Knudby, Y. Shen, Y. Liu, Mapping monthly air temperature in the Tibetan plateau from MODIS data based on machine learning methods, IEEE J. Sel. Top. Appl. Earth Obs. Rem. Sens. 11 (2018) 345–354, https://doi.org/10.1109/JSTARS.2017.2787191.
[66] H. Li, J. Lin, X. Lei, T. Wei, Compressive strength prediction of basalt fiber reinforced concrete via random forest algorithm, Mater. Today Commun. 30 (2022), 103117, https://doi.org/10.1016/j.mtcomm.2021.103117.
[67] S. Gao, Q. Zhan, C. Yang, H. Liu, The Diversified impacts of urban morphology on land surface temperature among urban functional zones, Int. J. Environ. Res. Publ. Health 17 (2020) E9578, https://doi.org/10.3390/ijerph17249578.
[68] B. Mota, M. Albergaria, H. Pereira, J. Silva, L. Gomes, Z. Vale, C. Ramos, Climatization and luminosity optimization of buildings using genetic algorithm, random forest, and regression models, Energy Inform. 4 (2021) 42, https://doi.org/10.1186/s42162-021-00151-x.
[69] Y. Ma, S. Zhang, K. Yang, M. Li, Influence of spatiotemporal pattern changes of impervious surface of urban megaregion on thermal environment: a case study of the Guangdong – Hong Kong – Macao Greater Bay Area of China, Ecol. Indicat. 121 (2021), 107106, https://doi.org/10.1016/j.ecolind.2020.107106.
[70] X. Yang, Z. Zhao, R. Hua, X. Su, L. Ma, Z. Chen, Simulation study on the influence of urban underground parking development on underlying surface and urban local thermal environment, Tunn. Undergr. Space Technol. 89 (2019) 133–150, https://doi.org/10.1016/j.tust.2019.03.023.
[71] A.-A. Faisal, A.-A. Kafy, A. Al Rakib, K.S. Akter, D. Md, A. Jahir, MdS. Sikdar, T. J. Ashrafi, S. Mallik, MdM. Rahman, Assessing and predicting land use/land cover, land surface temperature and urban thermal field variance index using Landsat imagery for Dhaka Metropolitan area, Environ. Chall. 4 (2021), 100192, https://doi.org/10.1016/j.envc.2021.100192.
[72] S. Pal, Sk Ziaul, Detection of land use and land cover change and land surface temperature in English Bazar urban centre, Egypt, J. Remote Sens. Space Sci. 20 (2017) 125–145, https://doi.org/10.1016/j.ejrs.2016.11.003.
[73] J. Peng, P. Xie, Y. Liu, J. Ma, Urban thermal environment dynamics and associated landscape pattern factors: a case study in the Beijing metropolitan region, Remote Sens. Environ. 173 (2016) 145–155, https://doi.org/10.1016/j.rse.2015.11.027.
[74] P.E. Osborne, T. Alvares-Sanches, Quantifying how landscape composition and configuration affect urban land surface temperatures using machine learning and neutral landscapes, Comput. Environ. Urban Syst. 76 (2019) 80–90, https://doi.org/10.1016/j.compenvurbsys.2019.04.003.
[75] Z. Wu, P. Dou, L. Chen, Comparative and combinative cooling effects of different spatial arrangements of buildings and trees on microclimate, Sustain. Cities Soc. 51 (2019), 101711, https://doi.org/10.1016/j.scs.2019.101711.
[76] H. Zhou, G. Tao, X. Yan, J. Sun, Influences of greening and structures on urban thermal environments: a case study in Xuzhou City, China, Urban For. Urban Green 66 (2021), 127386, https://doi.org/10.1016/j.ufug.2021.127386.
[77] D. Khamchiangta, S. Dhakal, Future urban expansion and local climate zone changes in relation to land surface temperature: Case of Bangkok Metropolitan Administration, Thailand, Urban Clim. 37 (2021), 100835, https://doi.org/10.1016/j.uclim.2021.100835.
[78] Q. Xie, Q. Sun, Monitoring thermal environment deterioration and its dynamic response to urban expansion in Wuhan, China, Urban Clim. 39 (2021), 100932, https://doi.org/10.1016/j.uclim.2021.100932.
[79] Y. Wang, Q. Zhan, W. Ouyang, How to quantify the relationship between spatial distribution of urban waterbodies and land surface temperature? Sci. Total Environ. 671 (2019) 1–9, https://doi.org/10.1016/j.scitotenv.2019.03.377.
[80] Y. Yang, J. Li, Study on urban thermal environmental factors in a water network area based on CFD simulation: a case study of Chengnan new district, Xiantao city,

Hubei Province, Environ. Technol. Innovat. 20 (2020), 101086, https://doi.org/10.1016/j.eti.2020.101086.

[81] T. Zhang, B. Hong, X. Su, Y. Li, L. Song, Effects of tree seasonal characteristics on thermal-visual perception and their influence on thermal comfort, Build. Environ. (2022), 108793, https://doi.org/10.1016/j.buildenv.2022.108793.

[82] R. Wang, H. Hou, Y. Murayama, A. Derdouri, Spatiotemporal analysis of land use/cover patterns and their relationship with land surface temperature in Nanjing, China, Rem. Sens. 12 (2020) 440, https://doi.org/10.3390/rs12030440.